



This is a repository copy of *The effect of stiffness on friction, surface strain and contact area of a sliding finger pad simulant.*

White Rose Research Online URL for this paper:

<https://eprints.whiterose.ac.uk/212299/>

Version: Published Version

Article:

Lee, Z.S., Maiti, R., Carré, M. et al. (1 more author) (2024) The effect of stiffness on friction, surface strain and contact area of a sliding finger pad simulant. *Tribology Letters*, 72 (2). 58. ISSN 1023-8883

<https://doi.org/10.1007/s11249-024-01861-5>

Reuse

This article is distributed under the terms of the Creative Commons Attribution (CC BY) licence. This licence allows you to distribute, remix, tweak, and build upon the work, even commercially, as long as you credit the authors for the original work. More information and the full terms of the licence here:

<https://creativecommons.org/licenses/>

Takedown

If you consider content in White Rose Research Online to be in breach of UK law, please notify us by emailing eprints@whiterose.ac.uk including the URL of the record and the reason for the withdrawal request.



eprints@whiterose.ac.uk
<https://eprints.whiterose.ac.uk/>



The Effect of Stiffness on Friction, Surface Strain and Contact Area of a Sliding Finger Pad Simulant

Zing Siang Lee¹ · Raman Maiti² · Matt Carré¹ · Roger Lewis¹

Received: 12 December 2023 / Accepted: 9 April 2024
© The Author(s) 2024

Abstract

This study investigates the frictional and surface strain behaviour of silicone hemispherical finger pad simulants with different stiffness during tribological interactions with a smooth glass plate. A novel contact area and strain measurement method employing a digital image correlation technique was employed to give new understanding of the pad behaviour during sliding. The frictional behaviour of the sliding finger pad simulant is dominated by the adhesion mechanism, with a small overall contribution from deformation, as suggested by the high principal strains at the edge of the contact area. The strain behaviour is also influenced by the magnitude of the normal force and the stiffness of the samples.

Keywords Finger pad simulant · Artificial finger pad · Synthetic finger pad · Friction · Strain · Digital image correlation

1 Introduction

Skin is a very interesting yet complicated material tribologically due to its heterogeneous intrinsic mechanical and material properties [1]. Humans use their hands and fingers to perceive objects, interact with the surroundings, and hold, grip and manipulate items as well. Therefore, the finger pad has become a strong focus of study in the field of biotribology [2]. Many factors affecting the friction of finger pad have been investigated, such as the normal load [3], sliding velocity [4], contact area [5], counterface roughness [6], skin structural properties [7], skin moisture condition [8], geometry of ridged surfaces [9, 10], counterface material types [11], existence of third body layer [12] and climate conditions [13]

The number of factors outlined above really emphasises the complexity of finger pad tribology. However, it is even more challenging to study the tribology of the finger pad because there is a large variation in finger pad skin between test participants [1]. Overcoming this is difficult, therefore, some studies have focussed on the development of synthetic material systems to simulate the human skin in terms of

mechanical properties, such as silicone rubbers and polyurethane in different fields and applications [14–17]. Nachman & Franklin further developed an artificial skin simulant that comprised of two layers of different materials [18]. The study highlight was the top layer of the skin simulant was made with hydrophilic silicone that could absorb water. Bostan et al. made a further attempt by integrating tissue-engineered skin with synthetic skin as a base layer [19]. However, these studies only looked into manufacturing skin as a flat piece of sample without considering the geometry of the finger and the ridges of the finger pad. Cutkosky & Wright laid the foundations for one of the earliest attempts in designing artificial fingers for robotic grasping [20]. This study investigated artificial finger pads with different geometrical tips ranging from pointed tips to curved flat tips. Since then, most studies focussed on using semi-spherical tips or samples with round curved end [21–23]. For instance, Xydas & Kao made a contact mechanics model based on a cylindrical finger with hemispherical-shaped end [21]. Han et al. also made artificial fingers that mimicked the whole finger including bone, nails and different radius at the tip of the artificial finger pad [24]. Although Yamada et al. did not make a cylindrical sample, but this study introduced the finger pad ridges into the samples (cuboid-shaped silicone block with controlled waviness on the contact surface) [25]. These studies worked towards perfecting the technology to manufacture a synthetic skin to mimic the human skin because it can be used as a better alternative test platform for

✉ Roger Lewis
roger.lewis@sheffield.ac.uk

¹ University of Sheffield, Sheffield, UK

² University of Loughborough, Loughborough, UK

finger pad experiments in research. In addition, it can also be applied to the development of robotic graspers in industry.

The experimental set-up in this study could measure the contact forces, surface strain and contact area (with some processing) of the sliding finger pad simulant simultaneously. Hemispherical finger pad simulants (to imitate human finger pad tip) with varied stiffness were made because many studies showed that the material stiffness played a significant role in the frictional behaviour of soft materials. Stiffness was linked to the measured data by performing a separate test that mapped the stiffness at the respective normal load the finger pad simulant could sustain with a flat counter-surface. This study presented the data with the respective stiffness instead of normal load to explore how the frictional and strain behaviour could be interpreted using stiffness.

2 Methodology

2.1 Finger Pad Simulants

The finger pad simulants in this study had a hemispherical shape and were made using room-temperature-vulcanizing (RTV) silicone rubber (Polycraft Silskin 10, MB Fibreglass, Northern Ireland). The “base” and “catalyst” of the silicone rubber were made with the ratio of 1:1. Then, “deadener” was added to soften the silicone. The amount of deadener added was varied to produce four batches of finger pad simulants with different stiffness. The respective deadener amount required for each batch was 0, 10, 15 and 20% of the combined volume of the “base” and “catalyst” silicone liquid.

The “base” and the “deadener” were first mixed after accurate measurement of the amount required to make the finger pad simulants. The “catalyst” was added to the mixture later because the curing process starts immediately when the “catalyst” was in contact with the “base”. The mixture was degassed before pouring into hemispherical-shaped moulds with a 6 mm radius. The whole silicone mixing process was completed within 15 min. A flat and rigid base was placed on top of the mould and the samples were left for a day to cure properly. Upon removal from the moulds, the hemispherical silicones were found to be securely adhered to the glass plates.

2.2 Experimental Set-Up

After the finger pad simulants were made, the first step was to characterise their stiffness behaviour. Then, the samples were used in the sliding tests. The samples were slid against a transparent flat plate to determine their friction behaviour. Imaging equipment was used simultaneously during the sliding tests to monitor the change in surface

strain of the finger pad simulants. The details of the stiffness test and sliding tests are discussed later in this section, whereas the details of the imaging equipment are shown in Sect. 2.3.

2.2.1 Stiffness Test

The stiffness of the finger pad simulants was measured using a compression test set-up, as illustrated in Fig. 1. Each simulant was placed and fixed under a flat stainless steel plate that was attached to a Mesmecin force gauge (Mesmecin, UK). A stainless steel flat plate was selected in the stiffness test to simulate the flat plate test condition in the sliding test.

The force gauge was attached to a manually operated test stand with a displacement transducer installed. The stainless steel plate was initially positioned close to the tip of the simulant barely touching it. The force gauge and the displacement transducer were zeroed before compressing the finger pad simulant. The normal load value was recorded with every 0.1 mm increment in displacement to allow a plot of normal load–displacement to be created. For every 0.1 mm compressive displacement, the finger pad simulant was allowed 10 s to stabilise before registering the normal load data. A polynomial equation could be fitted onto the force–displacement graph to estimate the this relationship. The stiffness equation was generated by deriving the force–displacement equation using the Newton–Raphson method. The stiffness–normal load graph was then plotted, as shown in Sect. 3.1, using the normal load and stiffness data generated from the displacement.

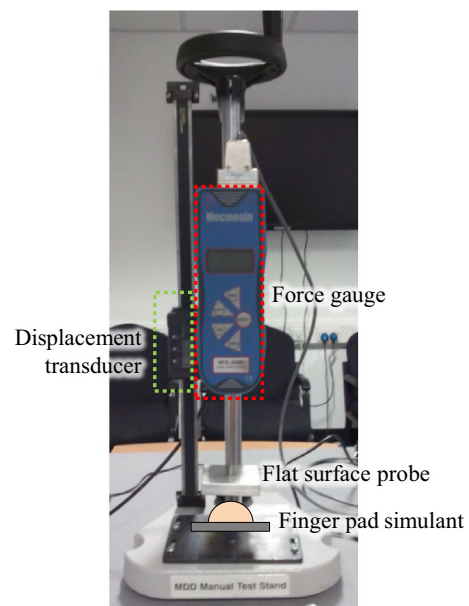


Fig. 1 Stiffness test set-up illustration

2.2.2 Sliding Test

The Human Interaction Sliding (HIS) rig was used in the sliding tests of the finger pad simulants. It is a bespoke rig made in The University of Sheffield that can both monitor the contact forces at the platform and controlling the sliding speed of the platform at the same time, while allowing monitoring of the finger pad/counterface surface to be carried out [26]. An illustration of the rig is shown in Fig. 2. The contact forces were measured using a 6-axis HE6×6 force plate (AMTI, USA). The moving platform was powered by a motorised leadscrew-driven linear slide (Reliance Precision Limited, UK) and the moving speed of the platform is controlled using LabView software.

Before the sliding test, the finger pad simulant was normally loaded against a glass plate using a bespoke loading device, as shown in Fig. 2b. The glass plate had an average thickness of $0.39 \pm 5 \mu\text{m}$ and average surface roughness, R_a , of $0.34 \mu\text{m}$. The sliding tests were performed at a range of

normal loads, which were 0.5, 1, 2 and 3 N. These ranges were used because this is the typical range when the full apparent contact area of the finger pad could be reached [5]. After the desired normal load was achieved, the glass plate was slid against the finger pad simulant at a constant speed of 0.26 mm/s. Slower speed was used because it would help in capturing the minor change in topography of the silicone simulant when it transitioned from undeformed to deformed state. The sliding was stopped after the platform had travelled for 75 s. The normal load was removed after approximately 20–30 s after the sliding had stopped to observe the recovery of the finger pad simulant.

2.3 3D Digital Image Correlation (DIC)

2.3.1 Sample Preparation and Experimental Set-Up

Digital image correlation (DIC) is an optical numerical full field measuring technique. It can be used to compute the

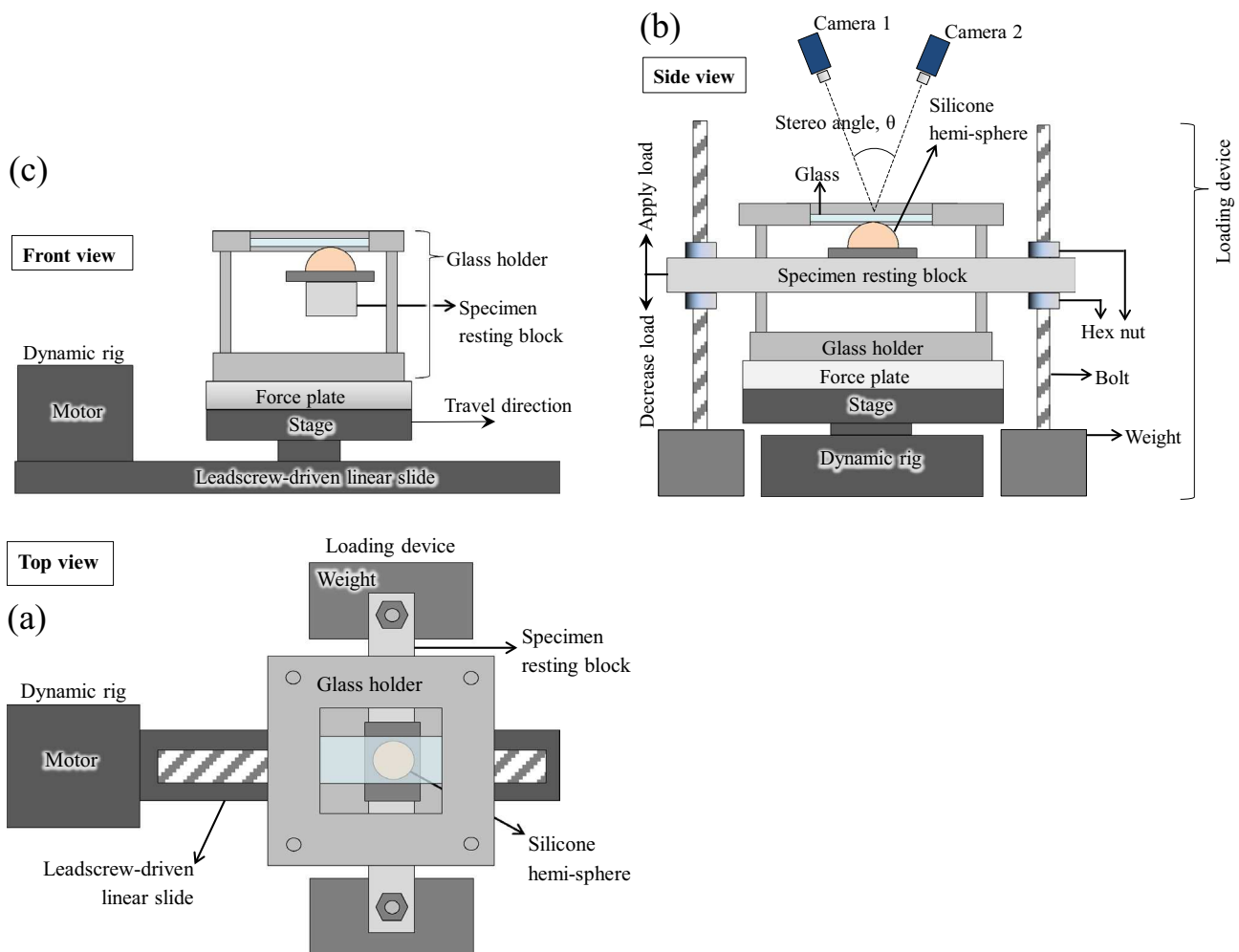


Fig. 2 a Top view and b and c side views of the sliding experiment set-up of the finger pad simulant

field of deformation on the surface of the finger pad simulant from the images of an undeformed and a deformed sample. The deformation is computed from the displacement tracking of random and unique speckles on the finger pad simulants, as shown in Fig. 3. A DIC system that uses one camera is 2D-DIC and two cameras is 3D-DIC. Both systems have the same working principle. However, the 3D-DIC is less sensitive to out-of-plane motions of the specimen [27] and more suitable to measure strain of a 3D sample. Therefore, the 3D-DIC system was selected in this study.

Using a 3D-DIC system requires sample preparation, camera set-up and calibration, acquisition of images and post-analysis [28, 29]. In this study, droplets of black water-based ink (crafters acrylic paint, DecoArt Inc., Stanford) were distributed randomly on the finger pad simulants by flicking the bristles of an unused toothbrush previously dipped with the ink. The resulting pattern was left to dry for approximately 1 h before testing.

Setting-up the camera required the adjustment of the stereo angle of the cameras, as shown in Fig. 2b, and the distance between the cameras, which were 30° [27] and 150 mm respectively in the current study. Two Pike F505B cameras (Allied Vision Technologies GmbH, Germany) equipped with monochromatic CCD sensor (Sony ICX625; $2/3''$; 2452×2054 pixels) and 50 mm lens objectives (XENOPLAN2.8/50–0902, Schneider, Kreuznach) were used.

After setting up the cameras, they were calibrated with a known grid size pattern of 11×10 with 2 mm spatial distance (calibration score: 0.064 pixels) by using VIC-3D

Digital Image Correlation software (version 7.2.1, Correlated Solutions, USA). The spatial pixel resolution was 0.013 mm/pixel, which resulted in a field of view of approximately $33 \times 27 \text{ mm}^2$ and an in-plane resolution of 0.009 mm^2 . At the image acquisition stage, five pairs of images were captured every second throughout the sliding experiment. Due to a relatively large speckle size, a subset size of 61×61 pixels was chosen for the correlation of images. The step size and the filter size were 7 and 15, respectively. The strain data were computed using Lagrange strain because this strain measure is more suitable to be used for materials undergoing large strain, such as the silicone samples used in this study. The noise levels of the principal strain data were approximately 0.3–0.4%. Details of the strain computation are explained in a study by Maiti et al. [30].

2.3.2 Determining Contact Area

As the 3D-DIC system could track the displacement of the speckles, it can also give the profile of the finger pad simulant. Therefore, the contact area of the finger pad simulant could be estimated by finding the boundary points in each plane, as shown in Fig. 4. A bespoke MATLAB algorithm was used to locate the coordinates of the boundary points by determining the change in gradient on the profile of the finger pad in Fig. 4b. 100 cross-sectional surface profiles, with a spacing of 0.15 mm, were analysed. The “ellipse best-fit” MATLAB function was then used to estimate the area of the contact from the boundary points.

Fig. 3 Speckles applied and the subset superimposed on **a** an undeformed and **b** a deformed finger pad simulant

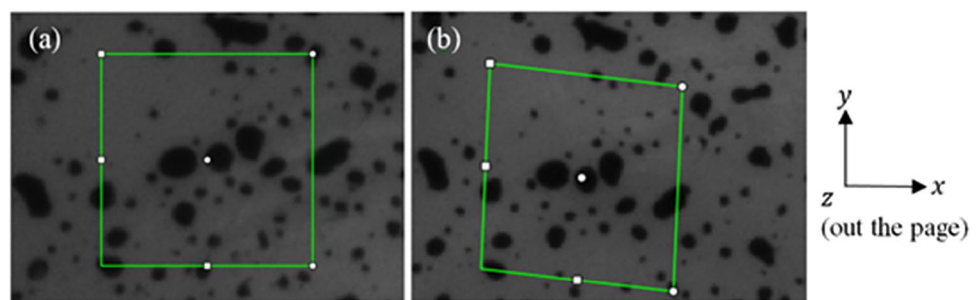
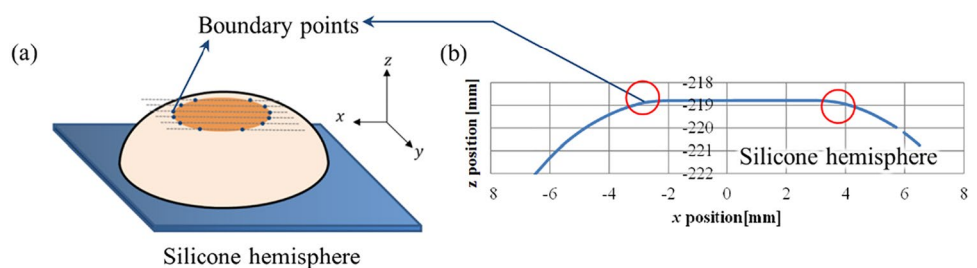


Fig. 4 **a** Illustration of the finger pad simulant in contact with glass plate and **b** the respective surface coordinates obtained from DIC data



3 Results

3.1 Stiffness of the Finger Pad Simulant

Figure 5a shows the normal load increased nonlinearly with increasing displacement, Tomlinson [31] observed a similar trend. As the deadener amount increased, less normal load was needed to reach a certain displacement. A fourth polynomial function was chosen as the equation of best fit because it has the highest R^2 number (> 0.99) across all finger pad simulants.

Stiffness is defined as the gradient of a load–displacement relationship. Figure 5b shows the stiffness of the finger pad simulants across a range of normal loads (see Sect. 2.3.1 for derivation method). This figure helps to estimate the stiffness of each sample at the respective normal load in the sliding tests in determining the relationship between friction/strain/contact area and stiffness in later sections.

3.2 Shear Force Before, During and After Sliding Test

There are three different phases in a typical sliding test in this study, as shown in Fig. 6. The first phase was before the sliding was started. The contact forces on the finger pad simulant were only composed of the normal load and no or minimal shear force. The second phase occurred during the sliding test. The contact force was composed of a steady friction force and normal load. Finger pad simulants with higher deadener amounts took a longer time to reach a steady friction force. The third phase was the recovery phase, which started when the sliding stopped. The shear force decreased as the finger pad simulant attempted to return to its original shape.

The normal load noticeably changed during the sliding test because the second moment area of the glass counterface was low and this is shown in Fig. 6. Nevertheless, the dynamic coefficient of friction was maintained at a steady value throughout the sliding test. Additionally, the largest bending angle occurring in the tests was 4° . Therefore, the bending effect is assumed to have a low impact on the resulting friction force. However, it should be noted that this might add uncertainty into the calculation of coefficient of friction as the uncertainty is amplified when calculating the coefficient of friction.

Figure 6 also shows that the dynamic friction force has larger noise level (peak to peak amplitude of 0.4 N) than the static friction force (peak to peak amplitude of 0.2 N). Although this is not the same as the stick–slip phenomena as observed in human finger pad sliding tests [4, 32], it could be related to an interesting phenomenon called the Schallamach waves [33]. This phenomenon was discovered when a hard hemispherical tip was slid against a layer of smooth soft rubber material, which resulted in the development of detachment waves in the sliding contact. Although the detachment did not occur in this study (see videos attached as supplement), the strain distribution in Fig. 8b could give a hint of how the stick–slip motion of a hemispherical silicone rubber would occur.

3.3 Relationship Between Stiffness and Friction

The coefficient of friction (CoF) of a finger pad simulant decreased when the pre-set normal load increased, as shown in Fig. 7a. As the amount of deadener in the finger pad simulant increased, the overall CoF increased as well due to increase in the contact area. Figure 7a also shows the relationship between the normal load applied and the contact area. The circle size indicates the size of the contact area.

Fig. 5 **a** Force–displacement graph of the finger pad simulants and **b** the respective stiffness vs normal load graph

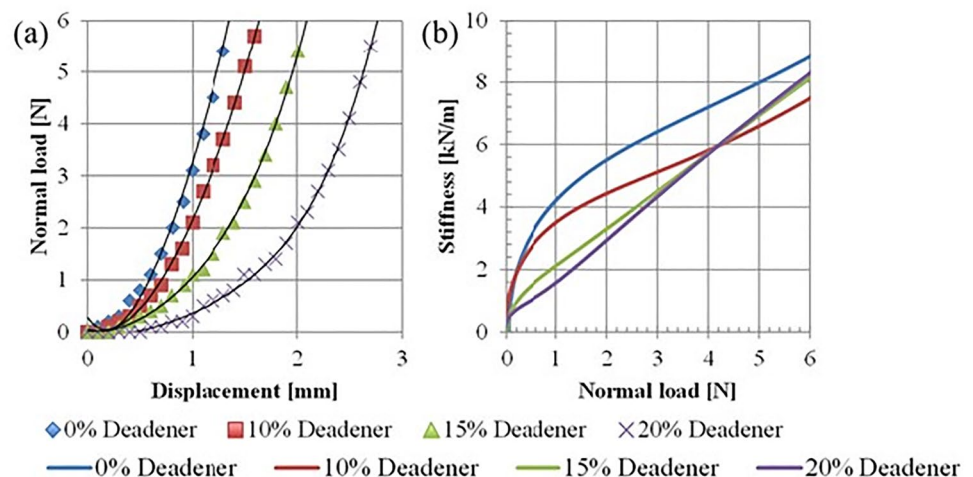


Fig. 6 The force behaviour of a finger pad simulant and the illustration of the bending mechanism of the glass plate

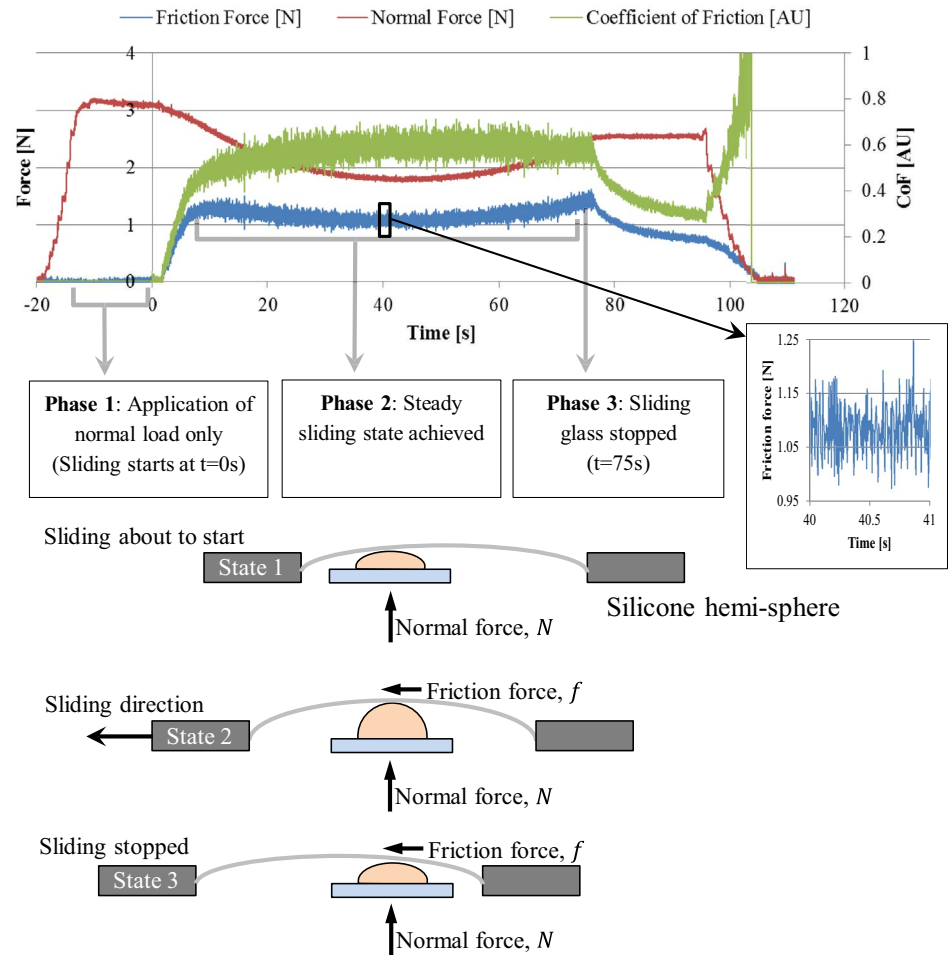
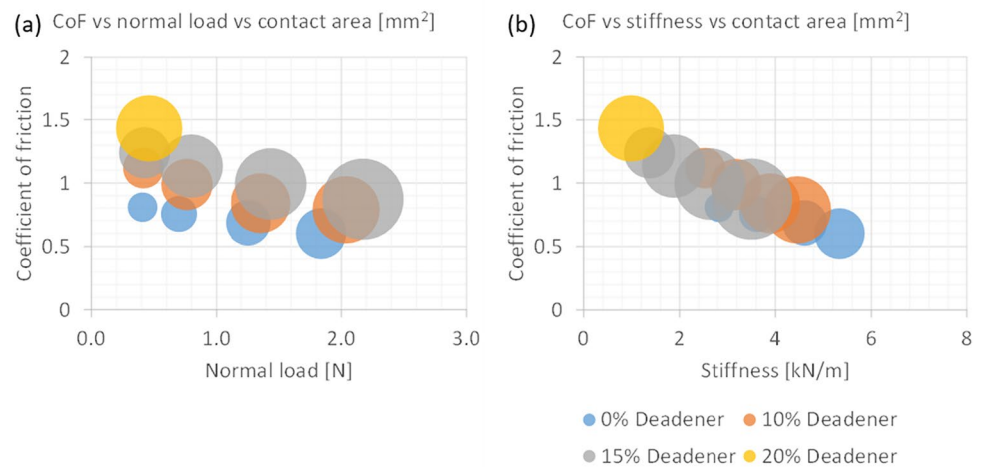


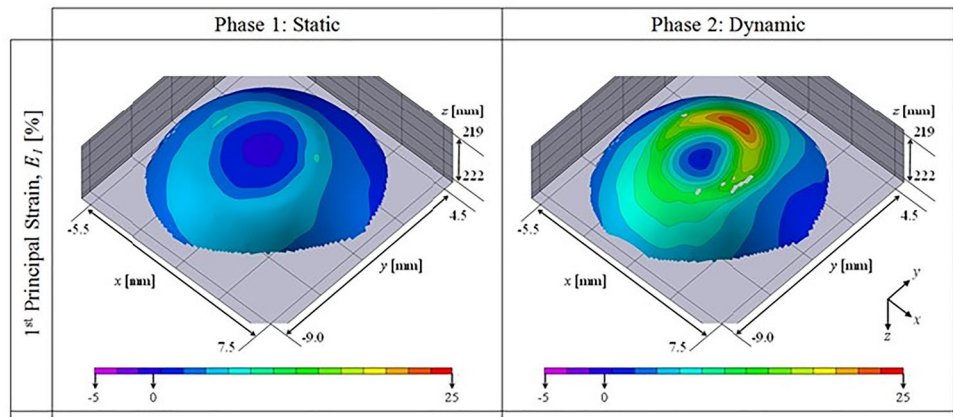
Fig. 7 The relationship of dynamic CoF and **a** normal load and **b** stiffness of finger pad simulants with the contact area (indicated by the circle size)



The CoF forms a linear relationship with the stiffness as it decreased linearly when the stiffness increased, as shown in Fig. 7b. In addition, the figure shows that any of the finger pad simulant would have similar CoF when the same stiffness level is achieved.

Figure 7b also shows the contact area increase linearly with the stiffness, which agrees with A. van Beek (2015). The relationship between contact area and stiffness of different finger pad simulants can be described using a family

Fig. 8 First principal strain, E_1 , of a finger pad simulant with 0% deadener in a 0.5N sliding test



of lines with different gradient, the detailed result is shown in Sect. 3.6.

3.4 General Surface Strain Behaviour

During the first phase of the sliding test, the surface strain was higher at the edge of the contact and virtually no surface deformation in the middle of the contact, as shown in Fig. 8a. The strain magnitude was also quite evenly distributed when there was no or minimal friction force at the contact. When the sliding started, the overall strain at the edge of the contact increased and the strain distribution shifted. For example, high first principal strain accumulated at the region along the sliding direction, as shown in Fig. 8b.

It should be noted that both principal strains were measured. Even though only the first principal strain is shown, this is sufficient to highlight the general surface strain behaviour of the finger pad simulant. The result of the second principal strain is provided as a supplement of this journal paper.

3.5 Relationship Between Stiffness and Strain

Figures 9 and 10 show the relationships between the first principal surface strain (averaged across the contact area) and the normal load or the respective stiffness of the finger pad simulant with 0% deadener and 15% deadener, respectively. It should be noted that the strain region where the finger pad simulant was in contact can be estimated using the technique to estimate contact area detailed in Sect. 2.3. The results of other finger pad simulants are accessible as supplementary data. The normal load in Figs. 9a and 10 was averaged in the steady sliding region. Therefore, the normal load decreased as mentioned in Sect. 3.2.

The results show that the surface strain increased proportionally as the stiffness increased in both the static and dynamic states. The increase in the amount of deadener added into the finger pad simulant prompted higher surface strain in response. Therefore, the relationship between strain, stiffness and the amount of deadener in the finger pad simulant can be described as a family of lines with different gradient. More experiments are needed to establish

Fig. 9 The relationship of averaged 1st principal strain, E_1 , and **a** normal load and **b** stiffness of a finger pad simulant with 0% deadener from static to dynamic state

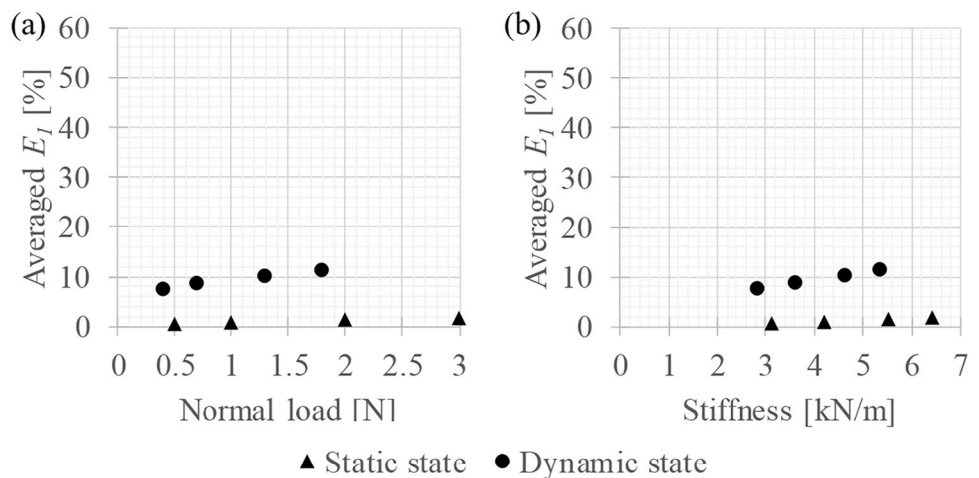
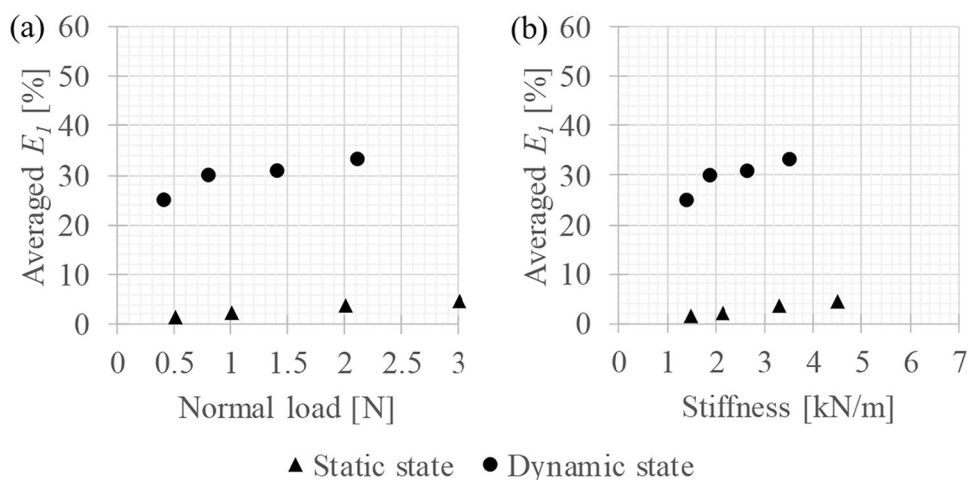


Fig. 10 The relationship of averaged 1st principal strain, E_1 , and **a** normal load and **b** stiffness of a finger pad simulant with 15% deadener from static to dynamic state



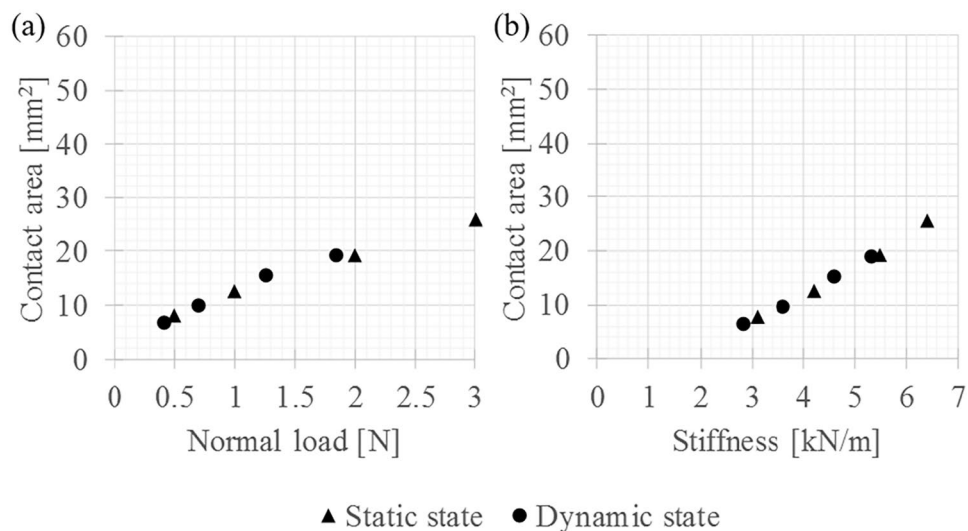
whether linear, polynomial or power is more suitable to describe the stiffness and stiffness relationship.

3.6 Relationship Between Stiffness and Contact Area

Figures 11 and 12 show the relationships between the contact area and the normal load or the respective stiffness of the finger pad simulant with 0% deadener and 15% deadener, respectively. The results showed that the contact area increased with the normal load.

The main difference between the two figures is the trend-line of the contact area between the static and dynamic state. The contact area was reduced as the normal load/stiffness was reduced in Fig. 11, whereas the contact area did not change much as the normal load/stiffness reduced, resulting in two different trend lines in Fig. 12.

Fig. 11 The relationship of contact area and **a** normal load and **b** stiffness of a finger pad simulant with 0% deadener from static to dynamic state



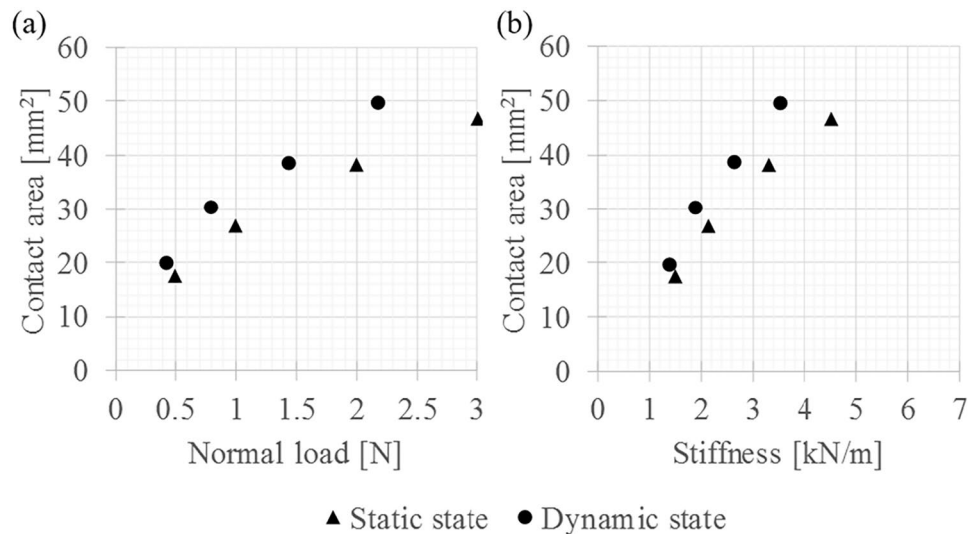
4 Discussions

4.1 Frictional and Strain Behaviour of Finger Pad Simulants

Previous studies showed that the coefficient of friction of the finger pad decreased with increasing normal load [1]. The frictional behaviour of the finger pad simulant made with silicone rubber followed the same trend. By varying the amount of deadener added into the samples, the overall CoF graph shifted up or down. This shows that the finger pad simulant with a hemispherical shape can be used as a simple imitation of the human finger pad in terms of frictional behaviour under different sliding conditions due to the wide range of CoF of the finger pad simulants.

The friction of a sliding finger is normally caused by a mix of adhesion and deformation [34]. Adhesion is caused by the formation and subsequent rupture of the interfacial

Fig. 12 The relationship of contact area and **a** normal load and **b** stiffness of a finger pad simulant with 15% deadener from static to dynamic state



junctions, while the deformation is due to the hysteresis or interlocking effects [1]. Hysteresis is caused by the incomplete recovery of the viscoelastic material during sliding that causes a skewed shift of the pressure distribution at the contact. Interlocking occurs when the asperities or roughness of the two objects match each other and interlock with each other as the two objects slide, leading to increase in friction [8].

The finger pad simulants also have both friction mechanisms. Adhesion is the predominant mechanism because the contact area is the main factor in the increase of friction as the results suggest in Sect. 3.6. The contact area increase was caused by the viscoelastic properties of the material increasing deformation in response to the increase of normal load. When more material is in contact, the higher the force required to break the molecular force at the contact between the two materials.

Hysteresis and interlocking are not considered as part of the friction mechanism in this study because both require a certain level of roughness to be able to contribute towards the overall friction [8]. The roughness of both the plate and the finger pad simulants in this study was approximately 0.34 μm . Tomlinson et al. discovered that the interlocking friction only contributes significantly when the height of the triangular ridge was 42.5 μm , whereas hysteresis from 250 μm .

The interesting feature about finger pad simulant is the “stickiness”. Ideally, the finger pad simulants should be made soft to mimic the softness of the human finger pad. In this study, the softer the finger pad simulant, the stickier the surface of the finger pad simulant. This means that bringing together two contact surfaces is easier than pulling them apart [35]. The stickiness of the finger pad simulant was evident during sliding as the strain distribution shifted with the sliding direction. This will become one of the main

challenges when designing a finger pad simulant because human finger pad is not as sticky.

Another interesting topic regarding the interaction between the finger pad simulant (rubber) and the glass plate is Schallamach waves. These occur due to the surface instabilities at the rubber surface [36]. Fukahori et al. (2010) summarised a list of general observation of a hard hemispherical tip sliding against a layer of rubber surface, which the relative sliding speed plays a significant role in the occurrence of detachment waves of the rubber at the contact [37]. Although there is an increase in the noise level of the dynamic friction force in comparison to the static friction force, the detachment waves were not found visually in this study. This is probably due to the sliding speed (0.26 mm/s) is lower than the critical sliding speed between the rubber and the glass [37]. However, the strain distribution at the contact might have a connection with the Schallamach waves because the waves normally occur at the edge of contact. It might be interesting to link the strain and Schallamach waves in future studies.

4.2 Role of Stiffness in the Frictional and Strain Behaviour

In order to study the effect of the stiffness on the friction and the strain behaviour of the finger pad simulants, the deadener was added in the silicone mixture to vary the mechanical properties of the finger pad simulants. The greater the amount of deadener in the silicone mixture, the less stiff the finger pad simulant sample is. Therefore, the finger pad simulants were described using “n%” amount of deadener in this study.

The purpose of the stiffness tests was to investigate if the friction and surface strain of the finger pad simulants could

be linked to the relative stiffness rather than the amount of the deadener in the samples.

The stiffness data could be used to describe the CoF without the limitation of the “amount of deadener” parameter. On the other hand, the strain between the finger pad simulants was still dependent on the “amount of deadener” in the finger pad simulants. Friction can be associated with the stiffness probably because the CoF was a bulk measurement at the contact. On the contrary, the surface strain was only a partial of the strain measurement, which the bulk occurred at the sub-surface of the finger pad simulants. Therefore, it is essential to investigate if the sub-surface strain can be derived from the surface strain in the future studies.

4.3 Development of Contact Area

As mentioned in Sect. 4.1, investigating the development of contact area of the finger pad simulants is important because more contact area means more adhesion. More adhesion also means more friction. The additional processing of the finger pad simulant profile (refer to Sect. 2.3 for more details) estimated the apparent contact area of the finger pad simulants. The results showed that the increase in normal load increased the contact area, which is in good agreement with the previous studies [1].

Liu et al. [15] and Delhayé et al. [38] found that the contact area of the finger pad decreases from static state to dynamic state. The decrease in contact area occurred in the tests involving finger pad simulants with 0% and 10% deadener (see Sect. 1.4 of the supplementary data). However, the finger pad simulant with 15% deadener experienced an increase in contact area during the tests. This can be explained using the adhesion hysteresis effect [35]. As the glass plate slid against the finger pad simulant, one contact region was in compression, and one was in tension. For a finger pad simulant with higher deadener, the material at the compressed side would tend to stay in contact because it lacked the additional force or energy to swiftly break away from the contact. As such, the dynamic and static contact would remain the same for finger pad simulants with low deadeners while the dynamic contact area will be significantly higher than static contact area for finger pad simulants with high deadener amount if the normal load could be kept constant throughout the sliding test.

5 Conclusions

This study investigated the frictional behaviour, surface strain behaviour and the development of contact area of finger pad simulants with different mechanical properties from the material stiffness perspective. The mechanical

properties were varied by controlling the amount of deadener added into the finger pad simulant. Measurements were carried out to determine the actual stiffness of each finger pad simulant at different normal loads.

The frictional behaviour of the finger pad simulant is similar to the finger pads based on previous studies [1], where the CoF decreases with the increase of normal load. The variation in the amount of deadener gave a range of CoF that would help in finding a suitable finger pad simulant to simulate different conditions of human finger pad. When the CoF was plotted against the stiffness of each finger pad simulant, the CoF decreased linearly with the stiffness disregarding the amount of deadener in the finger pad simulants. This means that a finger pad simulant can achieve certain friction as long as the stiffness is reached.

On the other hand, the surface strain behaviour is still dictated by the amount of deadener in the finger pad simulants. The results showed that the higher the amount of deadener, the more surface strain at the contact. However, the surface strain is just a part of the bulk strain. Nevertheless, studying surface strain helped in further understanding the friction mechanisms occurring at the contact, such as the hysteresis deformation and the adhesion hysteresis. In turn, the adhesion hysteresis also linked to the increase of the contact area when the finger pad simulant changed from the static state to the dynamic state.

Supplementary Information The online version contains supplementary material available at <https://doi.org/10.1007/s11249-024-01861-5>.

Acknowledgements The work was supported by the EPSRC Programme Grant “Friction: The Tribology Enigma” (EP/R001766/1) and the EPSRC Centre-to-Centre Grant “Tribology as an Enabling Technology” (TRENT) (EP/S030476/1). For the purpose of open access, the author has applied a Creative Commons Attribution (CC BY) license to any Author Accepted Manuscript version arising.

Author Contributions Z.S.L wrote the main manuscript text. Z.S.L and R.M. performed the experiments. All authors reviewed the manuscript.

Funding The authors have not disclosed any funding.

Data Availability The data can be made available on request.

Declarations

Conflict of interest There is no conflict of interest.

Open Access This article is licensed under a Creative Commons Attribution 4.0 International License, which permits use, sharing, adaptation, distribution and reproduction in any medium or format, as long as you give appropriate credit to the original author(s) and the source, provide a link to the Creative Commons licence, and indicate if changes were made. The images or other third party material in this article are included in the article’s Creative Commons licence, unless indicated otherwise in a credit line to the material. If material is not included in the article’s Creative Commons licence and your intended use is not permitted by statutory regulation or exceeds the permitted use, you will

need to obtain permission directly from the copyright holder. To view a copy of this licence, visit <http://creativecommons.org/licenses/by/4.0/>.

References

- Derler, S., Gerhardt, L.-C.: Tribology of skin: review and analysis of experimental results for the friction coefficient of human skin. *Tribol. Lett.* **45**, 1–27 (2012)
- Tomlinson, S.E., Lewis, R., Carré, M.J.: Review of the frictional properties of finger-object contact when gripping. *Proc. Inst. Mech. Eng. Part J: J. Eng. Tribol.* **221**(8), 841–850 (2007)
- Tomlinson, S.E., Lewis, R., Carré, M.J.: The effect of normal force and roughness on friction in human finger contact. *Wear* **267**, 1311–1318 (2009)
- Adams, M.J., Johnson, S.A., Lefèvre, P., Lévesque, V., Hayward, V., André, T., Thonnard, J.-L.: Finger pad friction and its role in grip and touch. *J. R. Soc. Interface.* **10**, 20120467 (2012)
- Liu, X., Carré, M.J., Zhang, Q., Lu, Z., Matcher, S.J., Lewis, R.: Measuring contact area in a sliding human finger-pad contact. *Skin Res. Technol.* **24**, 31–44 (2017)
- Tomlinson, S.E., Lewis, R., Ball, S., Yoxall, A., Carré, M.J.: Understanding the effect of finger-ball friction on the handling performance of rugby balls. *Sports Eng.* **11**, 109–118 (2009)
- Liu, X., Gad, D., Lu, Z., Lewis, R., Carre, M.J., Matcher, S.J.: The contributions of skin structural properties to the friction of human finger-pads. *Proc. IMechE Part J: J. Eng. Tribol.* **229**(3), 294–311 (2015)
- Tomlinson, S.E., Carré, M.J., Lewis, R., Franklin, S.E.: Human finger contact with small, triangular ridged surfaces. *Wear* **271**(9–10), 2346–2353 (2011)
- Tomlinson, S.E., Lewis, R., Liu, X., Texier, C., Carré, M.J.: Understanding the friction mechanisms between the human finger and flat contacting surfaces in moist conditions. *Tribology Letter* **41**, 283–294 (2011)
- Tomlinson, S.E., Lewis, R., Carré, M.J., Franklin, S.E.: Human finger friction in contacts with ridged surfaces. *Wear* **301**(1–2), 330–337 (2013)
- Kim, M.-S., Kim, I.-Y., Park, Y.-K., Lee, Y.-Z.: The friction measurement between finger skin and material surfaces. *Wear* **301**, 338–342 (2013)
- Bobjer, O., Johansson, S.-E., Piguet, S.: Friction between hand and handle. Effects of oil and lard on textured and non-textured surfaces; perception of discomfort. *Appl. Ergon.* **24**(3), 190–202 (1993)
- Hendriks, C.P., Franklin, S.E.: Influence of surface roughness, material and climate conditions on the friction of human skin. *Tribol. Lett.* **37**, 361–373 (2010)
- Gerhard, L.-C., Schiller, A., Müller, B., Spencer, N.D., Derler, S.: Fabrication, characterisation and tribological investigation of artificial skin surface lipid films. *Tribol. Lett.* **34**, 81–93 (2009)
- Morales Hurtado, M., Poppelman, M., Zeng, X., van Erp, P.E.J., Van Der Deide, E.: Tribological behaviour of skin equivalents and ex-vivo human skin against the material components of artificial turf in sliding contact. *Tribol. Int.* **102**, 103–113 (2016)
- Chen, J., Yang, H., Li, J., Chen, J., Zhang, Y., Zeng, X.: The development of an artificial skin model and its frictional interaction with wound dressings. *J. Mech. Behav. Biomed. Mater.* **94**, 308–316 (2019)
- Van Der Heide, E., Lossie, C.M., Van Bommel, K.J.C., Reinders, S.A.F., Lenting, H.B.M.: Experimental investigation of a polymer coating in sliding contact with skin-equivalent silicone rubber in an aqueous environment. *Tribol. Trans.* **53**(6), 842–847 (2010)
- Nachman, M., Franklin, S.E.: Artificial skin model simulating dry and moist in vivo human skin friction and deformation behaviour. *Tribol. Int.* **97**, 431–439 (2016)
- Bostan, L.E., Taylor, Z.A., Carre, M.J., Macneil, S., Franklin, S.E., Lewis, R.: A comparison of friction behaviour for ex vivo human, tissue engineered and synthetic skin. *Tribol. Int.* **103**, 487–495 (2016)
- Cutkosky, M.R., Wright, P.K.: Friction, stability and the design of robotic fingers. *Int. J. Robot. Res.* **5**(4), 20–37 (1986)
- Xydas, N., Kao, I.: Modeling of contact mechanics and friction limit surfaces for soft fingers in robotics, with experimental results. *Int. J. Robot. Res.* **18**(9), 941–950 (1999)
- Shao, F., Childs, T.H.C., Henson, B.: Developing an artificial fingertip with human friction properties. *Tribol. Int.* **42**(11–12), 1575–1581 (2009)
- Camillieri, B., Bueno, M.-A.: Artificial finger design for investigating the tactile friction of textile surfaces. *Tribol. Int.* **109**, 274–284 (2017)
- Han, H.-Y., Shimada, A., Kawamura, S.: Analysis of friction on human fingers and design of artificial fingers. In: Proceedings of the 1996 IEEE International Conference on Robotics and Automation, Minneapolis (1996)
- Yamada, D., Maeno T., Yamada, Y.: Artificial finger skin having ridges and distributed tactile sensors used for grasp force control. In: Proceedings of The 2001 IEEE/RSJ International Conference on Intelligent Robots and Systems, Maui (2001)
- Liu, X.: Understanding the effect of skin mechanical properties on the friction of human finger pads. Department of Mechanical Engineering, The University of Sheffield (2012)
- Reu, P.: Hidden components of 3D-DIC: triangulation and post-processing—part 3. *Exp. Tech.* **36**(4), 3–5 (2012)
- Reu, P.: Hidden components of DIC: calibration and shape function—part 1. *Exp. Tech.* **36**(2), 3–5 (2012)
- Reu, P.: Hidden components of 3D-DIC: interpolation and matching—part 2. *Exp. Tech.* **36**(3), 3–4 (2012)
- Maiti, R., Gerhardt, L.-C., Lee, Z.S., Byers, R.A., Woods, D., Sanz-Harrera, J.A., Franklin, S.E., Lewis, R., Matcher, S.J., Carré, M.J.: In vivo measurement of skin surface strain and sub-surface layer deformation induced by natural tissue stretching. *J. Mech. Behav. Biomed. Mater.* **62**, 556–569 (2016)
- Tomlinson, S.E.: Understanding the friction between human fingers and contacting surfaces. PhD Thesis, The University of Sheffield (2009)
- Derler, S., Rotaru, G.-M.: Stick-slip phenomena in the friction of human skin. *Wear* **301**(1–2), 324–329 (2013)
- Schallamach, A.: How does rubber slide? *Wear* **17**(4), 301–312 (1971)
- Adams, M.J., Briscoe, B.J., Johnson, S.A.: Friction and lubrication of human skin. *Tribol. Lett.* **26**, 239–253 (2007)
- Qian, L., Yu, B.: Adhesion hysteresis. In: Encyclopedia of tribology, pp. 29–32. Springer Link (2013)
- Khafidh, M., Setiyana, B., Jamari, J., Masen, M.A., Schipper, D.J.: Understanding the occurrence of a wavy wear track on elastomeric materials. *Wear* **412–413**, 23–29 (2018)
- Fukahori, Y., Gabriel, P., Busfield, J.J.C.: How does rubber truly slide between Schallamach waves and stick-slip motion? *Wear* **269**(11–12), 854–866 (2010)
- Delhaye, B., Barrea, A., Edin, B.B., Lefèvre, P., Thonnard, J.-L.: Surface strain measurements of fingertip skin under shearing. *J. R. Soc. Interface.* **13**, 20150874 (2016)

Publisher's Note Springer Nature remains neutral with regard to jurisdictional claims in published maps and institutional affiliations.